atoms

MDPI

Article

Experimental and Theoretical Electron Collision Broadening Parameters for Several Ti II Spectral Lines of Industrial and Astrophysical Interest

Lucía Isidoro-García [1,†], Isabel de Andrés-García [1,†], Juan Porro [2,†], Francisco Fernández [1,†] and Cristóbal Colón [1,2,*,†]

[1] E.T.S.I.D. Industrial, Universidad Politécnica de Madrid, Calle Ronda de Valencia 3, 28012 Madrid, Spain; lucía.isidoro@upm.es (L.I.-G.); mariaisabel.deandres@upm.es (I.d.A.-G.); francisco.fernandezm@upm.es (F.F.)
[2] E.T.S.I. Industrial, Universidad Politécnica de Madrid, Calle José Gutiérrez Abascal 2, 28006 Madrid, Spain; juanantonio.porro@upm.es
* Correspondence: cristobal.colon@upm.es
† These authors contributed equally to this work.

Abstract: A Q-switched Nd:YAG laser was focused on the Pb–Ti alloy samples in several laser-induced breakdown experiments in order to measure the Stark parameters of several spectral lines (58) of singly ionized titanium, including the 3504.89 Å and 3510.83 Å lines (where we achieved new experimental and theoretical values). The diagnostics of the laser-induced plasmas (electron density and electron temperature) were performed using Balmer's H alpha line (6562.7 Å). The temperatures were obtained by the Boltzmann plot technique with spectral lines of Pb I (after correction for its evident self-absorption). Subsequently, the calculations by the Griem approach of the Stark broadening parameters for several spectral lines were performed using the Gaunt factors proposed by van Regemorter and those proposed by Douglas H. Sampson. In the latter case, the values obtained were very close to the experimental values. This enables us to assume that the calculations performed for the spectral lines of Ti II, without experimental information, are more accurate using the Gaunt factors proposed by Sampson.

Keywords: atomic data; atomic processes

Citation: Isidoro-García, L.; de Andrés-García, I.; Porro, J.; Fernández, F.; Colón, C. Experimental and Theoretical Electron Collision Broadening Parameters for Several Ti II Spectral Lines of Industrial and Astrophysical Interest . *Atoms* **2024**, *12*, 35. https://doi.org/10.3390/atoms12070035

Academic Editor: Mehdi Ayouz

Received: 13 June 2024
Revised: 1 July 2024
Accepted: 4 July 2024
Published: 9 July 2024

1. Introduction

Knowing the properties of the chemical elements belonging to the iron period (Z = 21– 30), it is necessary to understand the core synthesis in the different types of supernovae: titanium (along with vanadium and scandium) is produced by the explosive combustion of silicon and oxygen in the SN phase of core collapse [1].

Information on the different titanium species (especially Ti I and Ti II) is needed to improve the accuracy of their stellar abundance determination. In the work of Wood et al. [2] on Ti II abundance in the photospheres of the Sun and metal-poor star HD 84937, the interest aroused by these species can be observed. In this work, the authors published improved Ti II atomic parameters for 364 spectral lines (present in the photospheres of the Sun and metal-poor star HD 84937) and the abundance determinations for 43 spectral lines (3263–5418 Å) present in the photospheres of the Sun. This is an important contribution, but one potential problem is that, in this last wavelength range, there are 377 Ti II lines (1683 if we include Ti I [3]). Some of these 377 lines are too close to those studied and even more intense. The presence of V II in the solar spectrum contributes to complicate the analysis and identification of the spectral lines. It is necessary to know how these lines can overlap with each other, affecting the published results, and for this it is necessary to analyze what their line broadening parameters are by collision with electrons.

In addition, titanium alloys are considered the most attractive metallic materials for industrial and biomedical applications. The Ti_6Al_4V alloy, developed before 1955, is the

best-known and most widely used titanium alloy. About half of the world's titanium production is for Ti_6Al_4V alloy applications. The Ti_6Al_4V alloy, due to its low density, high specific strength, and excellent performance, is one of the main materials used to manufacture aviation engine blades [4–6].

There are several experimental and theoretical papers on Ti II published recently due to the importance of titanium and its alloys in industry and astrophysics.

In 2016, using time-resolved laser-induced fluorescence, the experimental radiative lifetimes of six $3d^2(^3F)5s$ levels in singly ionized titanium with energy around 63,000 cm^{-1} and four odd-parity $3d^2(^3F)4p$ levels were measured by Lundberg et al. [7]. Combining the new 5s lifetimes with the branching fractions measured previously by Pickering et al. [8], they also reported 57 experimental log gf values for the transitions from the 5 s levels.

In 2022, a very complete theoretical work on the energy levels and transition probabilities for the Ti II ion was published by Alkallas et al. [9]. In addition to the calculations, a compilation of the experimental energy levels of Ti II collected at NIST appears in that paper, which represents great added value to the contributions of the paper.

In the bibliography, there is experimental and theoretical information related to the Stark broadening and displacement parameters for the lines of Ti II (Hermann et al. [10], Tankosi'c et al. [11], Sahal-Bréchot et al. [12], Manrique et al. [13], and in the Stark-B database [14]). Unfortunately, in our range of study, data have only been provided for 16 lines. The data gap should be compensated by our study.

The objective of this work is, therefore, to provide the broadening and displacement parameters of the profiles of 58 of these spectral lines, ranging between 3075–5418 Å and 9432.15 Å, to facilitate their identification and avoid possible errors and discrepancies.

Using the semiempirical formalism [15], the Stark broadening parameters (line widths and shifts) have been calculated for 58 singly ionized titanium spectral lines in this work. As in our work on ionized vanadium [16], we have performed two sets of calculations: some using the Gaunt factors provided by [15] and others using those provided by [17]. We have also conducted some experimental measurements that have served to contrast with the previous experimental data present in the literature and add new original experimental value in this work.

In the following sections, we present our experimental measurements and calculations of the final results for the Stark broadening parameters. For the lines of astrophysical interest on which we focus our experimental measurements, we show their Stark broadening parameters versus the temperature in a graphical representation. This representation includes the previous calculations, the final calculations, and the experimental measurements, both our own and those from the literature.

2. Experimental Setup

Different fluoride–lead-diluted titanium glass samples were prepared in our laboratory. The mixtures were heated at 700 °C in ceramic crucible in an air atmosphere for 12 h. The glass sample was not prepared with silica due to probable UV radiation silicate absorption. Fundamental wavelength (1.06 μm) of a Q-switched Nd:YAG laser (Quanta-Ray PRO-350 de Spectra-Physics) was focused on these samples in several laser-induced breakdown (LIB) experiments to obtain several spectral lines of singly ionized titanium (including the 3504.89 Å, 3510.83 Å, and 3587.13 Å spectral lines), neutral lead, and the Hα line. The energy per pulse (10 ns width) was measured at the target surface and was found to be 2.5 J. To avoid self-absorption of the titanium spectral lines, the titanium content in the samples was about 0.07–0.02%.

A picture of the experimental setup is shown in Figure 1 and is analogous to the one used by those authors in a recent work [16].

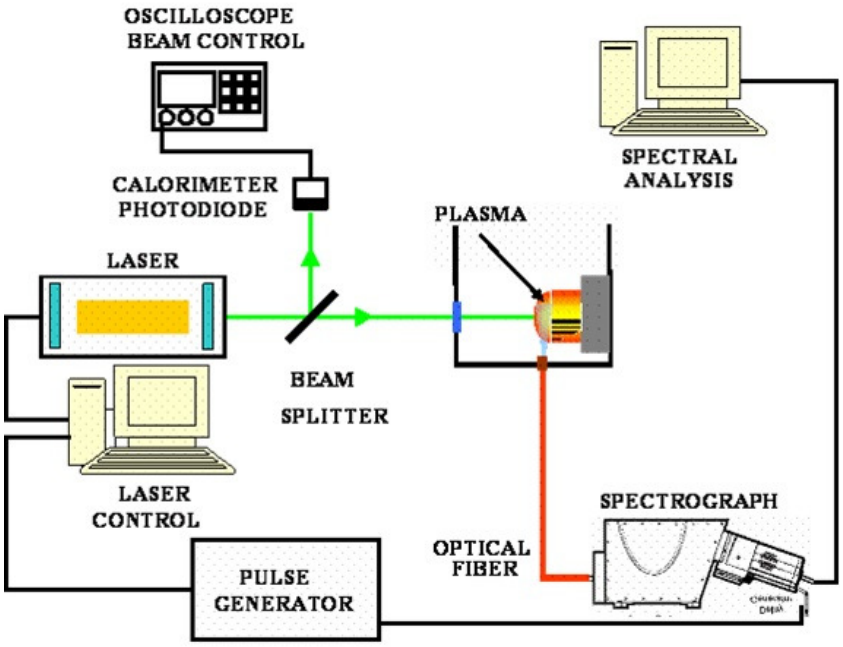

Figure 1. Photographic view of the LIB (and LSP) irradiation experimental setup.

A simple lens (f = 20 cm, biconvex) focuses the laser light on the sample. There is also a vessel with water supply system via hose connection, which provides a confined environment in permanent circulation (used only in LSP experiments) and a programmable 3D positioning system; the sample is over it, which allows us to control the distances between the lens and the sample and thus the spot size. The emission spectra were acquired using a spectrograph (Horiba Jobin Ybon FHR1000) equipped with a CCD camera (Andor, model iStar 334T). This camera's CCD is bidimensional, 1024 × 1024 pixels (26 × 26 μm^2 size per pixel), which allowed us to study the plasma spatially. The camera was time-controlled in both gate and delay with a maximum resolution of 100 ns. The spectrometer is equipped with a diffraction grating of 1800 groves/mm and covers a wavelength region from 200 to 700 nm. The emitted light was transferred to the spectrograph through a quartz fiber cable of 0.5 mm diameter. The data were taken by placing the optical fiber in the direction normal to the plasma emission and at a distance of 2 mm from the target surface (where the best signal-to-noise ratio was found). The spectra obtained were stored in a computer for further analysis. The analysis of the spectral lines was performed by fitting the observed line shapes to numerically generated Voigt profiles, which consist of the convolution obtained with the Lorentz and Gauss profiles. The identification of the lines was performed using the NIST Tables (Kramida et al., 2014) [3].

A procedure analogous to the one described in Moreno-Díaz et al. [18] was used to perform plasma diagnostics. Using the Stark width of the Hα line, we estimated the electron density numbers. In Figure 2, we display a sample of the Hα line on density was performed by fitting a Voigt profile to the experimental Halpha line emission. We have used the numerical facilities of the Microcal Origin program itself, where we analyze the spectral lines. This profile was analyzed two times: first by means of the tables for plasma diagnostics using the Lyman and Balmer hydrogen lines [19]; second, the following expression (1) (Ashkenazy et al. [20]) was used to obtain the electron number density, Ne, from the width of the H alpha line:

$$N_e = 8.02 \cdot 10^{12} \cdot \left(\frac{\blacksquare\lambda_{1/2}}{\mathrm{ff}_{1/2}} \right)^{3/2} cm^{-3} \quad (1)$$

where ■$\lambda_{1/2}$ is the FWHM (full width at half maximum) of the line in Å and $ff_{1/2}$ is half the width of the reduced Stark profiles in Å, and their precise values can be found in Kepple and Griem [21]. A value between 10,000 and 20,000 K was used (values compatible with the redshift of the line Hα) to choose the value of $ff_{1/2}$ from the table included in the above-mentioned paper.

The electron density values obtained for both procedures in our experiments for a delay from the laser pulse of 3 μs were compatibles of a value of $(2.31 \pm 0.60)\cdot 10^{17}$ cm^{-3}.

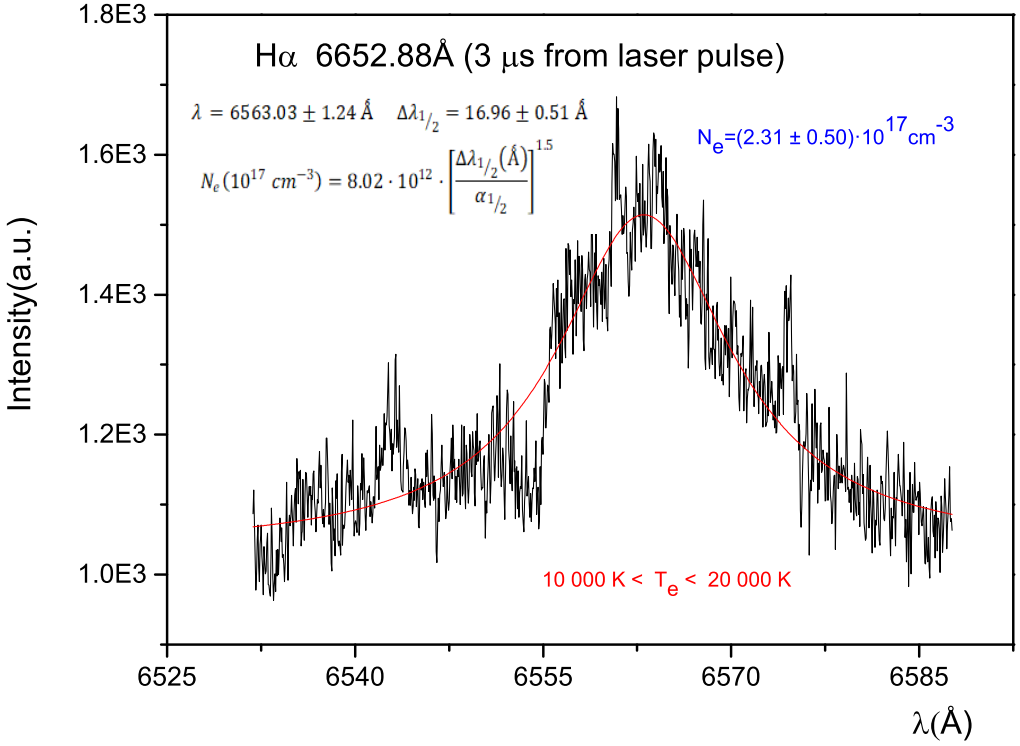

Figure 2. Fitting of a Voigt profile to the experimental Hα line emission from the plasma with a gate time of 500 ns at 3 μs delay time with a wavelength range from 6530 to 6590 Å.

The plasma temperatures at the different time windows were determinated from Boltzmann plots using several Pb I lines (see Figure 3) with upper level energies in the range 4.4–6.1 eV and well-known transition probabilities [3]. The resulting temperature before a self-absorption correction at 3.0 μs was (12,500 ± 1500) K. The self-absorption correction was obtained using the procedure described by [22]. In this procedure, we used our experimental lorentzian FWHM for the spectral lines and the experimental Stark broadening parameters of [23]. The resulting temperature after a self-absorption correction at 3.0 μs was (11,700 ± 1 500) K.

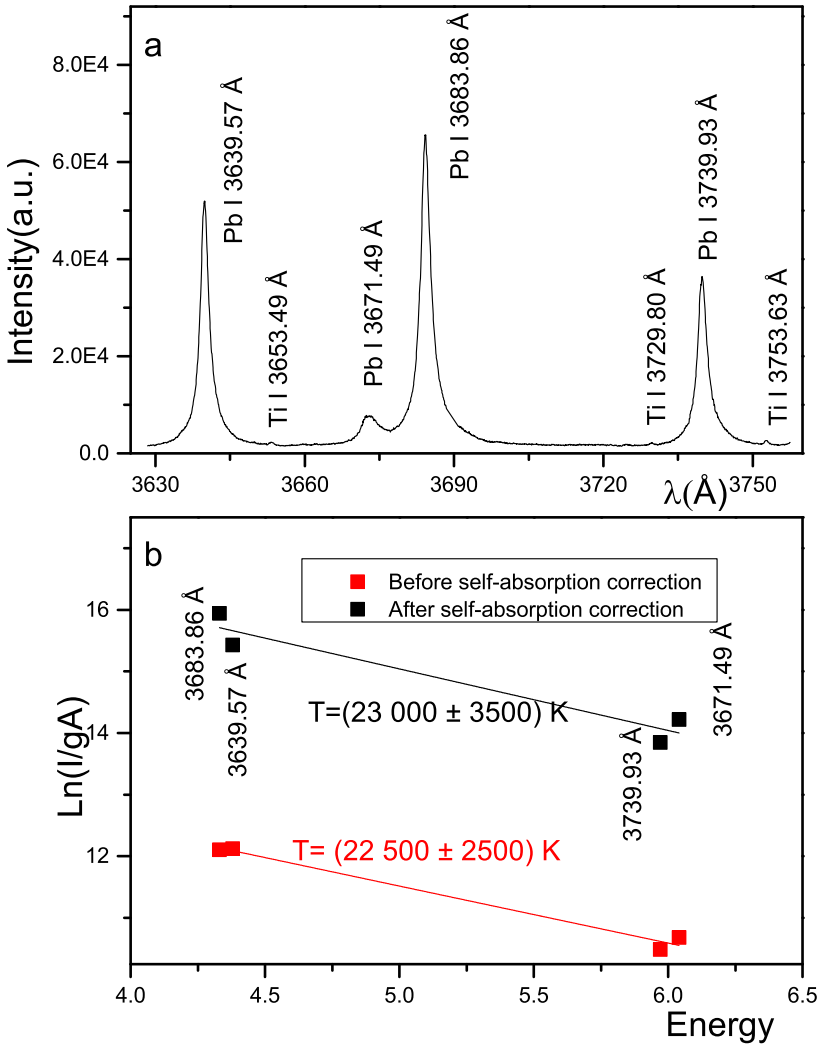

Figure 3. (**a**) Spectral emission of Ti–Pb sample at 3 μs after laser pulse in the 3630 at 3755 Å range. (**b**) Plasma temperature, at 3 μs after the laser pulse, estimated by a Boltzmann plot from the lines displayed in (**a**).

3. Theoretical Calculations

In the same way as in our previous studies, the Stark broadening parameters were calculated using the semiempirical Griem approximation [15]. The procedure involved Equations (2) and (3), where Griem incorporated Baranger's work [24]. The Stark line width (HWHM), ω_{se}, and shift, d, in angular frequency units, were determined using these equations. Initially, the effective Gaunt factors by [25] and van Regemorter [26], denoted as g_{se} and g_{sh}, were used.

$$\omega_{se} \approx 8\left(\frac{\pi}{3}\right)^{3/2}\frac{\hbar}{ma_0}N_e\left(\frac{E_H}{kT}\right)^{1/2}\times\left[\sum_{i'}|\langle i'|\vec{r}|i\rangle|^2 g_{se}\left(\frac{E}{\Delta E_{i'i}}\right)+\sum_{f'}|\langle f'|\vec{r}|f\rangle|^2 g_{se}\left(\frac{E}{\Delta E_{f'f}}\right)\right] \quad (2)$$

$$d \approx -8\left(\frac{\pi}{3}\right)^{3/2}\frac{\hbar}{ma_0}N_e\left(\frac{E_H}{kT}\right)^{1/2}\times \left[\sum_{i'}\left(\frac{\Delta E_{i'i}}{|\Delta E_{i'i}|}\right)|\langle i'|\vec{r}|i\rangle|^2 g_{sh}\left(\frac{E}{\Delta E_{i'i}}\right)-\sum_{f'}\left(\frac{\Delta E_{f'f}}{|\Delta E_{f'f}|}\right)|\langle f'|\vec{r}|f\rangle|^2 g_{sh}\left(\frac{E}{\Delta E_{f'f}}\right)\right] \quad (3)$$

Additionally, E_H and E = 3/2 kT represented the hydrogen ionization energy and the perturbing electron's energy, respectively, with k as the Boltzmann constant. The free electron density and electron temperature were denoted as N_e and T. The transitions' initial and final levels were labeled as i and f, with i' and f' representing the levels of Ti II with optical transitions corresponding to i and f. The energy differences between levels i' and i and levels f' and f were denoted as $\Delta E_{i'i}$ and $\Delta E_{f'f}$, respectively. The expressions of the type $|\langle i'|\vec{r}|i\rangle|^2$ are the square of matrix elements of the optical transitions.

To facilitate the spectroscopic use of our results, the conversion of angular frequency obtained in Griem's expressions into units of wavelength was essential. This conversion was achieved using the equation $\Delta\lambda = \omega_{se}\lambda^2/\pi c$. In this equation, $\Delta\lambda$ represents the Stark broadening (full width at half maximum, FWHM), λ denotes the wavelength, and c stands for the speed of light.

In this study, the matrix elements required for Equations (2) and (3) were derived using Cowan's code [27] based on energy levels from a previous work by Alkallas et al. [9]. Since our goal was a good set of matrix elements and not a very tight fit to the experimental energy levels, which is almost always achieved at the cost of worsening the fit of the transition probabilities (or, in other words, of the matrix elements), we have used in our calculations a reduced number of configurations, and, following Cowan's recommendations, we have not forced the fits more than 1%. We have considered the interaction of seven configurations of even parity, namely $3d^3$-$3d^2$4s-$3d^2$5s-$3d^2$6s-$3d^2$4d-$3d^2$5d-3d$4s^2$, and five configurations of odd parity, namely $3d^2$4p-$3d^2$5p-$3d^2$4f-3d4s4p-3d4s5p.

As in our previous work, we have performed two sets of calculations: the first using van Regemorter's Gaunt factors and the second using the calculations of these factors, expression (4), and the tables provided by [17].

$$g(x) = \frac{\sqrt{3}}{2\pi}\left\{\ln x + H_i\left[\left(\frac{\Delta E_{ii'}}{I_i}\right)^{r_i} + A_i\left(\frac{\Delta E_{ii'}}{I_i} - 1\right)\right]\left(1 - \frac{1}{x}\right)\right\} + \frac{\sqrt{3}}{2\pi}\left\{1.12\left(\frac{\Delta E_{ii'}}{I_i}\right)\frac{1}{x}\right\} \quad (4)$$

where I_i is the ionization energy for level i and the H_i, r_i, and A_i values were tabulated by Sampson and Zhang.

Both approaches coincide with high values of the Gaunt factor. The main difference is that Sampson's calculations provide lower values than the threshold value of 0.2 proposed by van Regemorter, which extends their validity to lower energy differences. It is because Sampson's expression for Gaunt's factors was derived from a complete study of collision cross-sections. His Gaunt factor was essentially an adaptation of these sections to Griem's expression and enables the use of sets of matrix elements calculated by Cowan's code.

4. Discussion

In Table 1, we show our experimental and theoretical values (using Sampson's Gaunt factors) for the Stark broadening parameters of four spectral lines of titanium II. In Figure 4, we show an example of our experimental measurements. By the simple inspection of Table 1, it can be seen that our values agree well with the experimental results of other authors.

Table 1. Ti II line widths (FWHM) and line shifts, ω (pm) and d (pm) at 13,000 K, normalized to $Ne = 10^{17}\text{cm}^{-3}$.

Wavelength	Transition Levels		This Work		Bibliography			
			ω	d	Ref [b]		Ref [c]	
λ (Å) [a]	Upper	Lower			ω	d	ω	d
3461.49	$3d\,^2 4p\,^4G^o_{9/2}$	$3d^3\,^4F_{7/2}$	13.03	−3.97	10.6 ± 1.6	3.6 ± 0.5	6 ± 1	−2 ± 1
3465.54	$3d^2 4p\,^2P^o_{1/2}$	$3d^2 4s\,^2P_{3/2}$	4.96	−1.89	10.5 ± 1.6	0.5 ± 0.1		
3504.89	$3d^2 4p\,^2G^o_{9/2}$	$3d^2 4s\,^2G_{9/2}$	20.83 16.8 * ± 3.6	−7.45	10.7 ± 1.6	0.8 ± 0.1	6 ± 1	0.4 ± 0.3
3510.83 **	$3d^2 4p\,^2G^o_{7/2}$	$3d^2 4s\,^2G_{7/2}$	16.73 16.9 * ± 3.8	−5.99				

Note: A negative shift is towards the red. [a] NIST. [b] Manrique et al., 2016 [13]. [c] Hermann et al., 2010 [10]. * Experimental value. ** New in the bibliography. Our experimental and theoretical values for the 3504.89 Å and 3510.83 Å lines are displayed at 11,700 K.

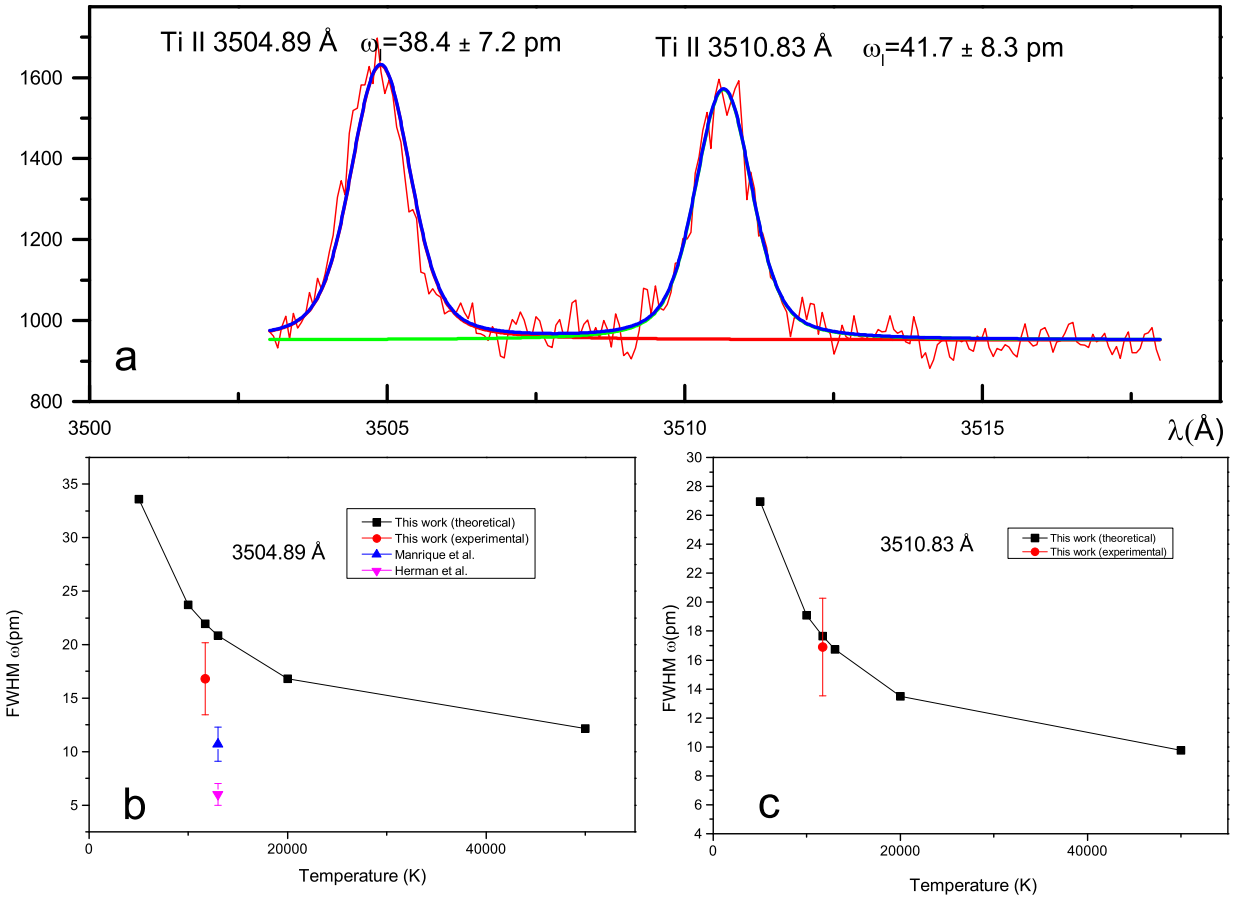

Figure 4. (**a**) Fitting of a Voigt profile to the experimental 3504.89 and 3510.83 Å emission lines from the plasma with a gate time of 500 ns at 3 µs delay time. (**b,c**) Stark width (FWHM) normalized to $Ne = 10^{17}$ cm^{-3} vs. temperature for 3504.89 and 3510.83 Å spectral lines of singly ionized titanium. On average, our measurements include a 30 percent error. Hermann et al. [10], Manrique et al. [13].

Table 2 presents the results obtained in our calculations using the Gaunt factors provided by van Regemorter and Sampson. The second column indicates the wavelength of each line and provides information about the multiplets of these lines' upper and lower levels. The third column provides the temperatures used in the calculations. In the remaining columns, we show, in pm, our theoretical values of the Stark line widths compared with the experimental values presented in the bibliography and normalized at an electron density of 10^{17} cm^{-3}. The calculations of Dimitrijevic's semiclassical approach

considering the classical trajectories instead of a quantum treatment of them appear in the last column of Table 2. The main results, that is, the values obtained with the Gaunt factors of van Regemorter, differ from the experimental values by a factor between 5 and 7, while the calculations performed with the expression proposed by Sampson and Zhang are very close to the experimental values. The raw comparison has problems because, in Dimitrijevic's calculations, there are no lines where the $3d^3$ level is involved, which is why there are gaps in that seventh column. We are waiting for new work from Dimitrijevic to compare with our results. It is observed that the calculations with the Gaunt factors of van Regemorter differ from the experimental values by a factor between 5 and 7, while the calculations performed with the expression proposed by Sampson and Zhang are very close to the experimental values of [13] (see as an example the lines of 3241.98 and 4443.80 Å) and our experimental value for the 3510.83 Å line. For this last line, both the experimental and theoretical values are new in the literature. We believe that this result should be extrapolated to the calculations conducted for the spectral lines in our study, from 3075.22 to 5418.76 Å, for many of which there are no experimental data. The shifts are too dependent on the transition probabilities used (there are contributions of both signs in Equation (3). To facilitate the reading of Table 2, we preferred not to include them in the text. We can provide them upon request.

Table 2. Ti II line widths (FWHM), ω (pm), normalized to $Ne = 10^{17}\text{cm}^{-3}$.

	Wavelength	**T (10^3 K)**	**ω (pm)**			
			This Work		**Bibliography**	
	λ (Å) [a]		**Reg**	**Samp**	**Ref c**	**Ref d**
1	3075.22	5	31.6	6.48		
Upper	$3d^2 4p\,^4D^o_{3/2}$	10	22.35	4.58		
Lower	$3d^2 4s\,^4F_{5/2}$	13	19.60	4.02	7.27	10.35
		20	15.8	3.24		
		50	10.01	2.3		
2	***3202.53***	5	71.97	14.75		
	$3d^2 4p\,^2F^o_{5/2}$	10	50.89	10.43		
	$3d^2 4s\,^2D_{3/2}$	20	35.99	7.38		
		50	22.7	5.41		
3	3218.26	5	81.43	16.69		
	$3d^2 4p\,^2G^o_{7/2}$	10	57.58	11.8		
	$3d^3\,^2H_{9/2}$	13	50.50	10.35	9.18	
		20	40.72	8.34		
		50	25.89	6.96		
4	3241.98	5	55.95	11.47		
	$3d^2 4p\,^4F^o_{3/2}$	10	39.56	8.11		
	$3d^2 4s\,^4F_{3/2}$	13	34.7	7.11	7.74	9.95
		20	27.97	5.73		
		50	17.69	3.63		

Table 2. *Cont.*

	Wavelength	T (10^3 K)	ω (pm)			
			This Work		Bibliography	
	λ (Å) [a]		Reg	Samp	Ref c	Ref d
5	***3276.772*** [b]	5	42.19	8.65		
	$3d^2 4p\,^4S^o_{3/2}$	10	29.83	6.12		
	$3d^3\,^4P_{5/2}$	20	21.09	4.32		
		50	13.38	3.27		
6	***3276.99*** [b]	5	70.48	0.1445		
	$3d^2 4p\,^2F^o_{7/2}$	10	49.83	0.1022		
	$3d^3\,^4F_{5/2}$	20	35.31	0.0744		
		50	22	0.0777		
7	***3278.288*** [b]	5	56.16	0.1151		
	$3d^2 4p\,^4D^o_{3/2}$	10	39.71	0.0814		
	$3d^2 4s\,^4P_{3/2}$	20	28.08	0.0576		
		50	17.75	0.0375		
8	***3278.92***	5	66.53	13.64		
	$3d^2 4p\,^2P^o_{3/2}$	10	47.04	9.64		
	$3d^2 4s\,^2D_{5/2}$	20	33.27	6.82		
		50	21.05	4.77		
9	3318.023 [b]	5	72.3	14.82		
	$3d^2 4p\,^4F^o_{7/2}$	10	51.13	10.48		
	$3d^3\,^4F_{5/2}$	13	44.84	9.19	9.21	
		20	36.15	7.41		
		50	22.87	4.69		
10	3409.808 [b]	5	54.78	11.23		
	$3d^2 4p\,^4G^o_{5/2}$	10	38.74	7.94		12.0
	$3d^4 4s\,^4F_{7/2}$	20	27.39	5.62		
		50	17.32	3.57		
11	***3452.465*** [b]	5	30.2	6.19		
	$3d^2 4p\,^2P^o_{1/2}$	10	21.35	4.38		
	$3d^2 4s\,^2P_{1/2}$	20	15.1	3.1		
		50	9.68	2.67		
12	***3533.854*** [b]	5	64.56	13.23		
	$3d^2 4p\,^2D^o_{3/2}$	10	45.65	9.36		
	$3d^2 4s\,^2P_{3/2}$	20	32.28	6.62		
		50	20.48	6.23		

Table 2. *Cont.*

	Wavelength	T (10^3 K)	ω (pm)			
			This Work		Bibliography	
	λ (Å) [a]		Reg	Samp	Ref c	Ref d
13	3535.407	5	88.12	18.06		
	$3d^2 4p\ ^2D^o_{5/2}$	10	62.31	12.77		
	$3d^2 4s\ ^2P_{3/2}$	13	54.65	11.2	12.3	
		20	44.06	9.03		
		50	27.96	8.66		
14	***3561.576*** [b]	5	97.22	19.93		
	$3d^2 4p\ ^4D^o_{5/2}$	10	68.75	14.09		
	$3d^2 4s\ ^2F_{5/2}$	20	48.64	10.07		
		50	30.43	9.26		
15	***3565.96***	5	26.43	5.42		
	$3d^2 4p\ ^2S^o_{1/2}$	10	18.69	3.83		
	$3d^2 4p\ ^4P_{3/2}$	20	13.22	2.71		
		50	8.41	2.47		
16	3706.21	5	51.93	10.65		
	$3d^2 4p\ ^2D^o_{3/2}$	10	36.72	7.53		
	$3d^3\ ^2D_{3/2}$	13	32.21	6.6	12.9	
		20	25.97	5.32		
		50	16.41	4.23		
17	***3741.638***	5	79.79	16.36		
	$3d^2 4p\ ^2D^o_{5/2}$	10	56.42	11.57		
	$3d^3\ ^2D_{5/2}$	20	39.9	8.18		
		50	25.22	6.49		
18	4307.866	5	71.71	14.7		
	$3d^2 4p\ ^4D^o_{3/2}$	10	50.71	10.4		
	$3d^3\ ^4P_{3/2}$	13	44.47	9.12	14.9	
		20	35.86	7.35		
		50	22.76	5.79		
19	***4316.794*** [b]	5	44.46	9.12		
	$3d^2 4p\ ^2P^o_{1/2}$	10	31.44	6.45		
	$3d^2 4s\ ^2P_{1/2}$	20	22.23	4.56		
		50	14.1	3.3		
20	***4320.95***	5	41.27	8.46		
	$3d^2 4p\ ^4D^o_{1/2}$	10	29.18	5.98		
	$3d^3\ ^4P_{3/2}$	20	20.64	4.23		
		50	13.1	3.51		

Table 2. *Cont.*

	Wavelength	T (10^3 K)	ω (pm)			
			This Work		Bibliography	
	λ (Å) [a]		Reg	Samp	Ref c	Ref d
21	***4330.238*** [b]	5	73.43	15.05		
	$3d^2 4p\,^2D^o_{3/2}$	10	51.92	10.64		
	$3d^2 4s\,^2P_{1/2}$	20	36.72	7.53		
		50	23.09	5.74		
22	***4337.91***	5	35.39	19.95		
	$3d^2 4p\,^2D^o_{3/2}$	10	25.03	14.11		
	$3d^2 4s\,^2D_{3/2}$	20	17.7	10.16		
		50	11.18	7.73		
23	***4421.938*** [b]	5	65.3	13.39		
	$3d^2 4p\,^2P^o_{3/2}$	10	46.17	9.47		
	$3d^2 4s\,^2P_{3/2}$	20	32.65	6.69		
		50	20.7	4.45		
24	4443.801 [b]	5	134.04	27.48		
	$3d^2 4p\,^2F^o_{5/2}$	10	94.78	19.43		
	$3d^2 4s\,^2D_{3/2}$	13	83.1	17.19	16.3	
		20	67.09	13.98		
		50	41.92	13.51		
25	***4444.554*** [b]	5	146.89	30.12		
	$3d^2 4p\,^2F^o_{7/2}$	10	103.87	21.29		
	$3d^3\,^2G_{7/2}$	20	73.56	15.46		
		50	45.84	16.54		
26	***4450.482*** [b]	5	153.61	31.49		
	$3d^2 4p\,^2F^o_{5/2}$	10	108.62	22.27		
	$3d^2 4s\,^2D_{5/2}$	20	76.88	15.99		
		50	48.1	14.98		
27	***4468.492***	5	131.05	26.86		
	$3d^2 4p\,^2F^o_{7/2}$	10	92.67	19		
	$3d^3\,^2G_{9/2}$	20	65.64	13.84		
		50	40.9	14.45		
28	***4469.151*** [b]	5	188.07	38.55		
	$3d^2 4p\,^4F^o_{7/2}$	10	132.98	27.26		
	$3d^2 4s\,^2D_{5/2}$	20	94.03	19.28		
		50	59.44	12.83		

Table 2. *Cont.*

	Wavelength	T (10^3 K)	ω (pm)			
			This Work		Bibliography	
	λ (Å) [a]		Reg	Samp	Ref c	Ref d
29	***4488.324*** [b]	5	216.77	44.44		
	$3d^2 4p\ ^2F^o_{7/2}$	10	153.28	31.42		
	$3d4s^{22}D_{5/2}$	20	108.59	22.87		
		50	69.46	18.08		
30	4501.26	5	117.09	24		
	$3d^2 4p\ ^2F^o_{5/2}$	10	82.8	16.97		
	$3d^{32}G_{7/2}$	13	72.6	15.04	18.6	
		20	58.62	12.25		
		50	36.5	13.25		
31	***4518.332*** [b]	5	105.42	21.61		
	$3d^2 4p\ ^4F^o_{3/2}$	10	74.54	15.28		
	$3d^2 4s\ ^2D_{3/2}$	20	52.71	10.81		
		50	33.32	7.29		
32	***4533.96***	5	113.23	23.21		
	$3d^2 4p\ ^2D^o_{5/2}$	10	80.07	16.41		
	$3d^{32}P_{3/2}$	20	56.65	11.76		
		50	35.74	10.44		
33	**4545.133** [b]	5	158.28	32.45		
	$3d^2 4p^2 G^o_{9/2}$	10	111.92	22.94		
	$3d^{3\,2}G_{7/2}$	20	79.14	16.23		
		50	49.96	11.77		
34	4549.22	5	214.83	44.04		
	$3d^2 4p^2 G^o_{9/2}$	10	151.91	31.14		
	$3d^{3\,2}H_{11/2}$	13	133.23	27.31	19.6	
		20	107.41	22.02		
		50	68.5	18.93		
35	4563.76	5	74.22	15.21		
	$3d^2 4p^2 D^o_{3/2}$	10	52.48	10.76		
	$3d^{3\,2}P_{1/2}$	13	46.03	9.44	16.5	
		20	37.15	7.81		
		50	23.76	6.29		
36	4571.97	5	174.49	35.77		
	$3d^2 4p^2 G^o{}_{7/2}$	10	123.38	25.3		
	$3d^{3\,2}H_{9/2}$	13	108.21	22.18	18.7	
		20	87.24	17.88		
		50	55.67	15.42		

Table 2. *Cont.*

	Wavelength	T (10^3 K)	ω (pm)			
			This Work		Bibliography	
	λ (Å) [a]		Reg	Samp	Ref c	Ref d
37	***4583.409*** [b]	5	114.06	23.38		
	$3d^2 4p\,^2F^o_{5/2}$	10	80.65	16.53		
	$3d^3\,^4P_{3/2}$	20	57.1	11.95		
		50	35.63	12.79		
38	***4589.94***	5	80.37	16.47		
	$3d^2 4p\,^2D^o_{3/2}$	10	56.83	11.65		
	$3d^3\,^2P_{3/2}$	20	40.22	8.45		
		50	25.73	7.07		
39	***4779.97***	5	51.88	10.64		
	$3d^2 4p\,^2S^o_{1/2}$	10	36.68	7.52		
	$3d^2 4s\,^2P_{1/2}$	20	25.94	5.32		
		50	16.44	4.27		
40	***4805.09***	5	68.9	14.12		
	$3d^2 4p\,^2S^o_{1/2}$	10	48.72	9.99		
	$3d^2 4s\,^2P_{3/2}$	20	34.45	7.06		
		50	21.84	5.68		
41	***4865.61*** [b]	5	132.2	27.1		
	$3d^2 4p\,^4G^o_{5/2}$	10	93.48	19.16		
	$3d^3\,^2G_{7/2}$	20	66.1	13.55		
		50	41.73	9.96		
42	***4874.009*** [b]	5	108.34	22.21		
	$3d^2 4p\,^2P^o_{1/2}$	10	76.61	15.7		
	$3d4s^2\ ^2D_{3/2}$	20	54.31	11.55		
		50	34.98	10.03		
43	***4911.194*** [b]	5	186.64	38.26		
	$3d^2 4p\,^2P^o_{3/2}$	10	131.98	27.06		
	$3d4s^2\,^2D_{5/2}$	20	93.57	19.92		
		50	60.41	17.52		
44	***5005.167*** [b]	5	98.23	20.14		
	$3d^2 4p\,^4D_{3/2}$	10	69.46	14.24		
	$3d^3\,^2D^o_{3/2}$	20	49.11	10.07		
		50	31.27	7.68		

Table 2. *Cont.*

	Wavelength	T (10^3 K)	ω (pm)			
			This Work		Bibliography	
	λ (Å) [a]		Reg	Samp	Ref c	Ref d
45	***5069.09*** [b]	5	201.31	41.27		
	$3d^2 4p\,^2D^o_{3/2}$	10	142.35	29.18		
	$3d4s^{2\,2}D_{5/2}$	20	100.92	21.48		
		50	64.68	19.91		
46	***5072.286*** [b]	5	249.94	51.24		
	$3d^2 4p\,^2D^o_{5/2}$	10	176.74	36.23		
	$3d4s^{2\ 2}D_{5/2}$	20	125.24	26.46		
		50	80.11	24.93		
47	***5154.06***	5	147.29	30.2		
	$3d^2 4p\,^2D^o_{5/2}$	10	104.15	21.35		
	$3d^{3\,2}D_{3/2}$	20	73.71	15.33		
		50	47.11	12.01		
48	***5185.902*** [b]	5	300.11	61.52		
	$3d^2 4p\,^2G^o_{7/2}$	10	212.21	43.5		
	$3d^2 4s\,^2G_{7/2}$	20	150.06	30.77		
		50	95.23	23.05		
49	***5188.68***	5	156.63	32.11		
	$3d^2 4p\,^2D^o_{5/2}$	10	110.75	22.7		
	$3d^{32}D_{5/2}$	20	78.38	16.29		
		50	50.14	12.94		
50	***5226.54***	5	105.75	21.68		
	$3d^2 4p\,^2D^o_{3/2}$	10	74.77	15.33		
	$3d^{32}D_{3/2}$	20	52.93	11.11		
		50	33.96	9.01		
51	***5336.786*** [b]	5	211.2	43.3		
	$3d^2 4p\,^2F^o_{7/2}$	10	149.34	30.62		
	$3d^{32}D_{5/2}$	20	105.77	22.22		
		50	66.26	23.2		
52	***5381.022*** [b]	5	158.84	32.56		
	$3d^2 4p\,^2F^o_{5/2}$	10	112.32	23.03		
	$3d^{32}D_{3/2}$	20	79.53	16.64		
		50	49.75	17.46		

Table 2. *Cont.*

	Wavelength	T (10^3 K)	ω (pm)			
			This Work		Bibliography	
	λ (Å) [a]		Reg	Samp	Ref c	Ref d
53	***5418.768*** [b]	5	169.1	34.66		
	$3d^2 4p\,^2F^o_{5/2}$	10	119.57	24.51		
	$3d^3\,^2D_{5/2}$	20	84.65	17.69		
		50	53.06	18.55		
54	***9432.151*** [b]	5	667.96	136.94		
	$3d^2 4p\,^2F^o_{7/2}$	10	472.32	96.83		
	$3d^3\,^2F_{7/2}$	20	334.46	70.59		
		50	209.25	80		

[a] NIST . [b] Line of Ti II in the Sun. Ref c Manrique et al., 2016 [13]. Ref d Tankosić et al., 2001 [11].

5. Conclusions

In this work, we have performed Stark broadening measurements of the 3504.89 and 3510.83 Å spectral lines of singly ionized titanium, which confirmed the previous measurements of 2016 obtained by others authors. Also, we have calculated the Stark broadening parameters, using the procedure suggested by Sampson to obtain the Gaunt factors, of 54 spectral lines of Ti II. In this way, we have obtained results very close to the experimental values for 12 of these spectral lines. They have allowed us to assume that the calculations performed for 42 lines ranging between 3075 and 5419 Å (present in the photospheres of the Sun and the metal-poor star HD 8493), and without experimental information, are accurate using the Gaunt factors proposed by Sampson.

Author Contributions: All authors have participated in all stages of the work. All authors have read and agreed to the published version of the manuscript.

Funding: This research received no external funding.

Informed Consent Statement: Not applicable.

Data Availability Statement: All data required are available in this paper or in the cited bibliography. The shifts are too dependent on the transition probabilities used (there are contributions of both signs in Equation (3). To facilitate the reading of Table 2, we preferred not to include them in the text. We can provide them upon request.

Acknowledgments: Work partly supported by MINECO (Spain; Grants MAT2015–63974-C4–2-R and PID2019–104351GB-C21).

Conflicts of Interest: The authors declare no conflicts of interest.

References

1. Woosley, S.E.; Weaver, T.A. The Evolution and Explosion of Massive Stars. II. Explosive Hydrodynamics and Nucleosynthesis. *Astrophys. J. Suppl. Ser.* **1995**, *101*, 181. https://doi.org/10.1086/192237.
2. Wood, M.P.; Lawler, J.E.; Sneden, C.; Cowan, J.J. Improved Ti II log(gf) values and abundance determinations in the photospheres of the Sun and metal-poor star HD 84937. *Astrophys. J. Suppl. Ser.* **2013**, *208*, 27. https://doi.org/10.1088/0067-0049/208/2/27.
3. Kramida, A.; Ralchenco, Y.; Reader, J. NIST ASD Team (2013) NIST Atomic Spectra Database (v.5.3). 2013. Available online: http://physics.nist.gov/asd (accessed on 1 January 2024).
4. Yadav, M.; Misra, A.; Malhotra, A.; Kumar, N. Design and analysis of a high-pressure turbine blade in a jet engine using advanced materials. *Mater. Today Proc.* **2020**, *25*, 639–645. https://doi.org/10.1016/j.matpr.2019.07.530.
5. Moayedee, Y.; Nikzad, L.; Fakhraei, O.; Paykar, Z.; Zekavat, E. Improvement of mechanical, biological, and electrochemical properties of Ti6Al4V alloy modified with Nb and Ag for biomedical applications. *J. Alloys Compd.* **2024**, *972*, 172736. https://doi.org/10.1016/j.jallcom.2023.172736.

6. Warzanskyj, W.; Angulo, I.; Cordovilla, F.; Díaz, M.; Porro, J.; García-Beltrán, A.; Cabeza, S.; Ocaña, J. Analysis of the thermal stability of residual stresses induced in Ti-6Al-4 V by high density LSP treatments. *J. Alloys Compd.* **2023**, *931*, 167530. https://doi.org/10.1016/j.jallcom.2022.167530.
7. Lundberg, H.; Hartman, H.; Engström, L.; Nilsson, H.; Persson, A.; Palmeri, P.; Quinet, P.; Fivet, V.; Malcheva, G.; Blagoev, K. Oscillator strengths for high-excitation Ti ii from laboratory measurements and calculations. *Mon. Not. R. Astron. Soc.* **2016**, *460*, 356–362. https://doi.org/10.1093/mnras/stw922.
8. Pickering, J.C.; Thorne, A.P.; Perez, R. Oscillator Strengths of Transitions in Ti II in the Visible and Ultraviolet regions. *Astrophys. J. Suppl. Ser.* **2001**, *132*, 403. https://doi.org/10.1086/318958.
9. Alkallas, F.H.; Abu El Maati, L.; Ben Nessib, N.; Dimitrijević, M.S. Energy levels of the singly ionized titanium: Ti II ion. *Astron. Nachrichten* **2022**, *343*, e210059. https://doi.org/10.1002/asna.20210059.
10. Hermann, J.; Thomann, A.L.; Boulmer-Leborgne, C.; Dubreuil, B.; De Giorgi, M.L.; Perrone, A.; Luches, A.; Mihailescu, I.N. Plasma diagnostics in pulsed laser TiN layer deposition. *J. Appl. Phys.* **1995**, *77*, 2928–2936. https://doi.org/10.1063/1.358708.
11. Tankosi'c, D.; Popovic, L.C.; Dimitrijevic, M.S. Electron-impact Stark broadening parameters for Ti II and Ti III spectral lines. *At. Data Nucl. Data Tables* **2001**, *77*, 277–310. https://doi.org/10.1006/adnd.2000.0856.
12. Sahal-Bréchot, S.; Dimitrijević, M.S.; Moreau, N.; Nessib, N.B. The STARK-B database VAMDC node: A repository for spectral line broadening and shifts due to collisions with charged particles. *Phys. Scr.* **2015**, *90*, 054008. https://doi.org/10.1088/0031-8949/90/5/054008.
13. Manrique, J.; Aguilera, J.A.; Aragón, C. Experimental Stark widths and shifts of Ti ii spectral lines. *Mon. Not. R. Astron. Soc.* **2016**, *462*, 1501–1507. https://doi.org/10.1093/mnras/stw1641.
14. Sahal-Brechot, S.; Dimitrijevic, M.; Nessib, N.B.; Moreau, N. STARK-B. 2020. Available online: http://stark-b.obspm.fr/index.php/contact (accessed on 1 January 2024).
15. Griem, H.T. Semiempirical formulas for the Electron-Impact widths and shifts of isolated ion lines in plasmas. *Phys. Rev.* **1968**, *165*, 258–266. https://doi.org/10.1103/physrev.165.258.
16. de Andrés-García, I.; Isidoro-García, L.; Fernández, F.; Porro, J.; Colón, C. Influence of Gaunt factors on the calculation of the Stark broadening parameters for 56 spectral lines of Vii with high industrial and astrophysical interest. *Mon. Not. R. Astron. Soc.* **2023**, *523*, 2146–2157. https://doi.org/10.1093/mnras/stad1555.
17. Sampson, D.H.; Zhang, H.L. Semiempirical Formulae for Electron Impact Excitation and Ionization of Hydrogenic Ions. *apj* **1988**, *335*, 516. https://doi.org/10.1086/166945.
18. Moreno-Díaz, C.; Alonso-Medina, A.; Colón, C.; Porro, J.; Ocaña, J. Measurement of plasma electron density generated in an experiment of Laser Shock Processing, utilizing the Halpha-line. *J. Mater. Process. Technol.* **2016**, *232*, 9–18. https://doi.org/10.1016/j.jmatprotec.2016.01.026.
19. Gigosos, M.; Cardeñoso-Payo, V. New plasma diagnosis tables of hydrogen Stark broadening including ion dynamics. *J. Phys. B At. Mol. Opt. Phys.* **1999**, *29*, 4795. https://doi.org/10.1088/0953-4075/29/20/029.
20. Ashkenazy, J.; Kipper, R.; Caner, M. Spectroscopic measurements of electron density of capillary plasma based on Stark broadening of hydrogen lines. *Phys. Rev. A* **1991**, *43*, 5568–5574. https://doi.org/10.1103/PhysRevA.43.5568.
21. Kepple, P.; Griem, H.R. Improved Stark Profile Calculations for the Hydrogen Lines Hα, Hβ, Hγ, and Hδ. *Phys. Rev.* **1968**, *173*, 317–325. https://doi.org/10.1103/PhysRev.173.317.
22. El Sherbini, A.; El Sherbini, T.; Hegazy, H.; Cristoforetti, G.; Legnaioli, S.; Palleschi, V.; Pardini, L.; Salvetti, A.; Tognoni, E. Evaluation of self-absorption coefficients of aluminum emission lines in laser-induced breakdown spectroscopy measurements. *Spectrochim. Acta Part B At. Spectrosc.* **2005**, *60*, 1573–1579. https://doi.org/10.1016/j.sab.2005.10.011.
23. Alonso-Medina, A. Experimental determination of the Stark widths of Pb I spectral lines in a laser-induced plasma. *Spectrochim. Acta Part B At. Spectrosc.* **2008**, *63*, 598–602. https://doi.org/10.1016/j.sab.2008.03.002.
24. Baranger, M. General Impact Theory of Pressure Broadening. *Phys. Rev.* **1958**, *112*, 855–865.
25. Seaton, M.J. The Theory of Excitation and Ionization by Electron Impact. In *Proceedings of the Atomic and Molecular Processes*; Seaton, M.J., Bates, D.R., Eds.; Academic Press Inc.: New York, NY, USA, 1962; pp. 374–420.
26. van Regemorter, H. Rate of Collisional Excitation in Stellar Atmospheres. *Astrophys. J.* **1962**, *136*, 906. https://doi.org/10.1086/147445.
27. Cowan, R. *The Theory of Atomic Struture and Spectra*; University of California Press: Berkeley, CA, USA, 1981; p. 57. https://doi.org/10.1063/1.2915135.